remote sensing

MDPI

Article

Physiological and Hyperspectral Responses of Individual European Beech Trees to Drought Stress: A Pilot Study During a Compound Drought and Heatwave Event

Karolina Sakowska [1], Luca Belelli Marchesini [2], Michele Dalponte [2], Mustafa Elfahl [1], Mirco Rodeghiero [2], Francesca Ugolini [3], Stefania Pilati [2], Loris Vescovo [2], Luis Alonso Chorda [4,5] and Chiara Torresan [1,*]

1 Institute of BioEconomy, National Research Council, 38098 San Michele all'Adige, Italy; karolina.sakowska@cnr.it (K.S.); mustafa.elfahl@ibe.cnr.it (M.E.)
2 Research and Innovation Center, Fondazione Edmund Mach, 38098 San Michele all'Adige, Italy; luca.belellimarchesini@fmach.it (L.B.M.); michele.dalponte@fmach.it (M.D.); mirco.rodeghiero@fmach.it (M.R.); stefania.pilati@fmach.it (S.P.); loris.vescovo@fmach.it (L.V.)
3 Institute of BioEconomy, National Research Council, 50019 Sesto Fiorentino, Italy; francesca.ugolini@cnr.it
4 Faculty of Agriculture and Forestry, University of Helsinki, 00790 Helsinki, Finland; luis.alonsochorda@helsinki.fi
5 Mediterranean Center for Environmental Studies, 46980 Paterna, Spain; alonso@ceam.es
* Correspondence: chiara.torresan@cnr.it

Highlights

What are the main findings?

- Water-stressed beech exhibited up to 70% reductions in photosynthesis and 35% reductions in chlorophyll content under severe drought conditions.
- Red-edge hyperspectral indices successfully detected individual-tree stress; the traditional NDVI failed.

What are the implications of the main findings?

- Early drought stress impairs photosynthesis before visible symptoms appear, underscoring the need for proactive monitoring systems for forest management.
- Airborne remote sensing enables stress detection in beeches facing increasing climate extremes.

Abstract

European beech is a species of both ecological and economic relevance in Europe. However, its high sensitivity to drought poses a significant risk amid increasing climate extremes. This study aimed to evaluate the physiological and spectral responses of beech to drought stress, combining in situ leaf-level measurements with hyperspectral remote sensing data. We set up the experiment in an Alpine European beech forest in northern Italy, which included three water treatments: control, water stress, and irrigation. Physiological data (i.e., leaf gas exchange and chlorophyll content), alongside airborne hyperspectral remote sensing data, were collected from 20 to 29 July 2022 during a compound drought and heatwave (CDHW) event. Water-stressed trees exhibited significantly reduced photosynthetic rates, lower photosystem II efficiency, and higher non-photochemical quenching, indicating impaired photosynthetic performance. Water-stressed beech exhibited up to 70% reduced photosynthesis and 35% lower leaf chlorophyll content under severe drought conditions. Hyperspectral vegetation indices, particularly the RENDVI, CIRE, and SPRI, successfully detected stress status. This exploratory study, based on an intensive analysis of four trees, demonstrates the feasibility of integrating physiological measurements with hyperspectral

Academic Editor: Ran Meng

Received: 5 December 2025
Revised: 25 January 2026
Accepted: 26 January 2026
Published: 3 February 2026

remote sensing to detect drought-stress signatures in European beech at the individual-tree level, establishing a methodological framework for more extensive future research.

Keywords: gas exchange; non-photochemical quenching; chlorophyll content; airborne hyperspectral imaging; spectral indices; LiDAR

1. Introduction

The increasing frequency of extreme climate events is placing substantial pressure on many mountain environments [1]. Extreme events—defined as rare weather occurrences within the current climate regime [2,3]—include heatwaves, i.e., prolonged periods of abnormally high temperatures [4], and droughts, i.e., sustained periods of below-normal water availability [5]. When a heatwave and drought occur simultaneously (i.e., intersect) in the same region, the event is defined as a compound drought and heatwave (CDHW) event. CDHW can cause severe damage to forests, often exceeding the impacts of individual events [6].

Despite its humid climate, classified as Dfc (subarctic climate) and Dfb (warm-summer humid continental climate) under the Köppen–Geiger climate classification [7], the European Alpine mountain region is experiencing drought [8], which was already projected to increase in occurrence in the future in past studies [9], especially in its southern areas [8]. Moreover, heatwaves are expected to become more frequent in the latter part of the 21st century [10,11].

These extreme climatic events have significant consequences for tree species adapted to pronounced seasonality and short vegetative periods, such as Norway spruce (*Picea abies* (L.) Karst.), silver fir (*Abies alba* Mill.), Scots pine (*Pinus sylvestris* L.) and dwarf mountain pine (*Pinus mugo* Turra), which represent the main species of Alpine coniferous forests [12]. These ecosystems are particularly vulnerable to drought, mainly in July and August, when reduced precipitation [13] and high temperatures coincide with high water demand, resulting in water stress [14]. Also, thermophilous deciduous forests, i.e., forests dominated by deciduous or semi-deciduous thermophilous species, mainly downy oak (*Quercus pubescens* Willd.) [12], are affected by drought [15,16] and by rising temperatures, even without changes in precipitation patterns [17]. Compared to *Quercus* species, the European beech (*Fagus sylvatica* L.) in mountainous beech forests or in mixed forests with coniferous species, such as silver fir and/or Norway spruce, has been shown to be more vulnerable to drought, especially during the summer months [18].

Heatwaves and drought events affect key metabolic processes associated with photosynthesis and respiration, impair nutrient uptake, and alter nutrient partitioning and competition patterns [19]. At the leaf level, extreme-heat events reduce photosynthetic activity and increase photooxidative stress. When combined with a limited water supply, they reduce stomatal conductance and transpiration, a mechanism that helps to cool leaves [20]. In addition, this increases resistance to CO_2 diffusion in intercellular air spaces [19], further limiting photosynthetic efficiency. At the whole-plant level, heat stress exacerbated by drought can decrease growth, leaf development, and leaf area, inducing shifts in biomass allocation and ultimately leading to tree mortality. Therefore, there is an urgent need to enhance our understanding of how trees respond to such events, especially in drought-sensitive species such as European beech.

The development of remote sensing-based monitoring strategies for trees capable of detecting stress signals [21,22] is very important, and spectral vegetation indices (SVIs) are widely used to describe vegetation properties, such as photosynthetic activity and

canopy structure [23]. SVIs can exploit reflectance patterns in the visible (VIS, 380–750 nm), near-infrared (NIR, 700–1100 nm), and shortwave infrared (SWIR, 1100–2500 nm) domains, which are primarily determined by leaf pigments, structure, and water content, respectively. Several SVIs have proven particularly valuable for monitoring forest stress. The normalised difference vegetation index (NDVI) [24] has been a foundational tool since the 1970s, but it saturates in dense canopies. Red-edge indices, such as the red-edge normalised difference vegetation index (RENDVI) and the red-edge chlorophyll index (CIRE), address this limitation and more effectively estimate chlorophyll content and leaf area index (LAI) in dense vegetation [25]. The photochemical reflectance index (PRI) provides insight into physiological function by reflecting xanthophyll cycle dynamics, serving as a proxy for photosynthetic light-use efficiency and stress status [26–28]. Finally, water-sensitive indices, such as the normalised water index (NWI), enable the detection of changes in leaf water content, which are critical for identifying drought stress [29].

However, interpreting these spectral signals requires ground-truth validation through physiological measurements. In situ photosynthetic light-response curves, which quantify net photosynthesis across gradients of photosynthetically active radiation (PAR), provide essential validation for linking spectral data to physiological function [30]. Similarly, leaf chlorophyll measurements provide an independent ground-based reference and represent a key indicator of photosynthetic capacity and plant stress status.

The primary objective of this study was to explore the crown spectral response of European beech individuals across three levels of drought stress, combining aerial remote sensing with physiological observations. In more detail, we aimed to address the following research questions: (1) How do CDHW events affect physiological and biochemical parameters of European beech trees growing in mountainous regions of the northeastern Italian Alps? (2) How does the canopy reflectance of European beech trees vary in water-stressed trees compared to non-stressed ones? (3) Can individual-tree stress responses be detected through hyperspectral indices measured at the crown level? To answer these questions, a combined aerial and ground measurement campaign was conducted in the summer of 2022 in the mountain beech forest on trees subjected to three different water treatments.

Given the logistical complexity of combining intensive crown-level physiological measurements with airborne hyperspectral acquisitions, we conducted an exploratory study on a limited number of intensively monitored trees. In view of these constraints, we framed the above research questions as exploratory hypotheses for a pilot test, acknowledging that broader inferences about species responses require future studies with greater replication.

2. Materials and Methods

2.1. Study Site and Experimental Setup

The study site is a 4 ha European beech forest located in the Cembra Lisignago municipality (Trento Province, Italy, 46°12′9″N; 11°12′35″E) at an elevation of 1270 m a.s.l. The forest is part of the 'Nitrogen Forest Experiment' facility, which is integrated into the Emphasis and AnaEE ERIC European research infrastructures [31]. Although the Cembra forest stand is very heterogeneous in terms of species composition, the subplot of European beech stand considered in this study is almost pure (87% of trees belonging to the same species), with a density of 796 trees per hectare, a mean diameter at breast height (DBH) of 18.9 cm (with the minimum inventoried DBH 3 cm), and a mean height of 15.3 m (values refer to 2022). The stand includes a limited presence (9%) of Norway spruce and a minor presence of silver fir, silver birch (*Betula pendula* Roth), Scots pine, European larch (*Larix decidua* L.) and rowan (*Sorbus aucuparia* L.). The location of all trees was georeferenced in previous forest inventory surveys using a total station. The stand grows on an acidic brown soil (Cambisol, WRB 2015) over a porphyry (Rhyolite) bedrock. Beech forests

that grow in this type of soil and bedrock have relatively poor water retention capacity compared to many other beech forests. Cambisols developed on porphyry/rhyolite typically have a coarser texture than those on different parent materials, which reduces their water-holding capacity.

In spring 2022, four European beech trees of similar size and competitive position, occupying comparable microsites in flat areas of the study site, were selected. The trees were assigned to three experimental conditions: one control and two water treatments. Specifically, two trees were not subjected to any treatment, grew under natural ambient conditions and served as control trees (CO1 and CO2); one tree was subjected to water-stress manipulation by placing a plastic tarp over approximately 144 m^2 of the soil surface around the stem (distance of 6 m from the trunk) starting on 21 May 2021, which prevented rainwater infiltration and thereby limited root water availability (ST1); one tree was irrigated during the summer 2022 measurement campaign to simulate optimal water status (IR1), receiving supplemental water on 25 July (1000 litres), 26 July (500 litres), and 28 July (500 litres). All trees, regardless of treatment, were also exposed to a CDHW event in the summer of 2022 (Section 2.2).

The main dendrometric features of the investigated trees are reported in Table 1.

Table 1. Features of the investigated trees (values refer to spring 2022). DBH is the diameter at breast height. Mean tree crown diameter was calculated as the average of the crown diameters measured in the four cardinal directions.

Treatment (Tree Type)	Treatment Acronym	Tree Code	DBH (cm)	Tree Height (m)	Mean Tree Crown Diameter (m)
Control (control trees, untreated and facing the CDHW event of 2022)	CO	CO1	23.0	20.0	7.0
		CO2	30.5	19.5	6.5
Irrigation (irrigated tree, facing the CDHW event of 2022 and supplemented with water)	IR	IR1	29.5	19.2	5.2
Water stress (water-stressed tree, facing the CDHW event of 2022 in addition to water stress imposed through a longer-term manipulation experiment)	ST	ST1	27.3	20.1	5.2

The field measurement campaign was carried out from 20 to 29 July 2022. During this period, in situ physiological data, airborne hyperspectral remote sensing data, and UAV–LiDAR data were collected. To reach the upper sunlit leaves of the tree crown, two aerial work platforms were used: a truck-mounted lift with a telescopic boom extendable up to 21 m and a spider lift with a telescopic boom extendable up to 27 m (Figure 1).

2.2. Climate Data and Weather Conditions During the Field Campaign

During the summer of 2022, Europe experienced the most severe CDHW event in recent history [32–34]. The event was particularly intense across the Iberian Peninsula, France, Italy, the northwest Balkans, Germany, the Netherlands, Poland, and Scandinavia [35]. Record-breaking temperatures were recorded, and drought conditions persisted throughout the summer [33]. In the Alpine region, an exceptionally low-snowfall winter, which further intensified the soil moisture deficit [36,37], exacerbated the severity of the CDHW event. In detail, the eastern Alpine region of Italy experienced daily temperature anomalies of up to 2.5 °C during the third week of July 2022 compared with the median values from long-term observations (1993–2021) [33].

Figure 1. The two mobile elevating work platforms used for ecophysiological measurements: the truck-mounted lift (**A**) and the spider lift (**B**).

We used daily data from the meteorological station of the Meteotrentino network of the Autonomous Province of Trento, located in the Cembra Lisignago municipality at 652 m a.s.l., to compare temperature and precipitation patterns in 2022 with the reference period 1993–2021. Figure 2A shows the mean daily temperature for 2022 (red line) together with the median (black line) and the 25th and 75th percentiles (grey area) of the daily temperature from the 1993–2021 series. Around DOY 200, a marked increase in daily temperatures was observed, coinciding with the July 2022 heatwave. Regarding precipitation, Figure 2B shows that the cumulative rainfall up to DOY 250 was below the 25th percentile of the 1993–2021 series, indicating a significant precipitation deficit.

The study site is equipped with a 26-metre-high meteorological tower that collects standard meteorological data (air temperature and relative humidity, atmospheric pressure, precipitation, and incoming solar radiation). According to data collected by the on-site weather station, the first part of the field campaign, from 20 to 24 July 2022, was characterised by an average maximum daily temperature of 27.1 °C and no precipitation. In the second part of the field campaign, i.e., 25–29 July 2022, the total precipitation amounted to 31.4 mm, with rainfall events on the 25th, 26th, 27th and 29th of July (8.0, 1.8, 17.2 and 4.4 mm, respectively), and the average maximum daily temperature was 23.5 °C. Considering the entire campaign period, from 20 to 29 July 2022, the mean daily air temperature and relative humidity were 18.7 °C and 78.5%, respectively. The mean values of soil temperature and soil moisture were 15.1 °C and 20.8%, respectively.

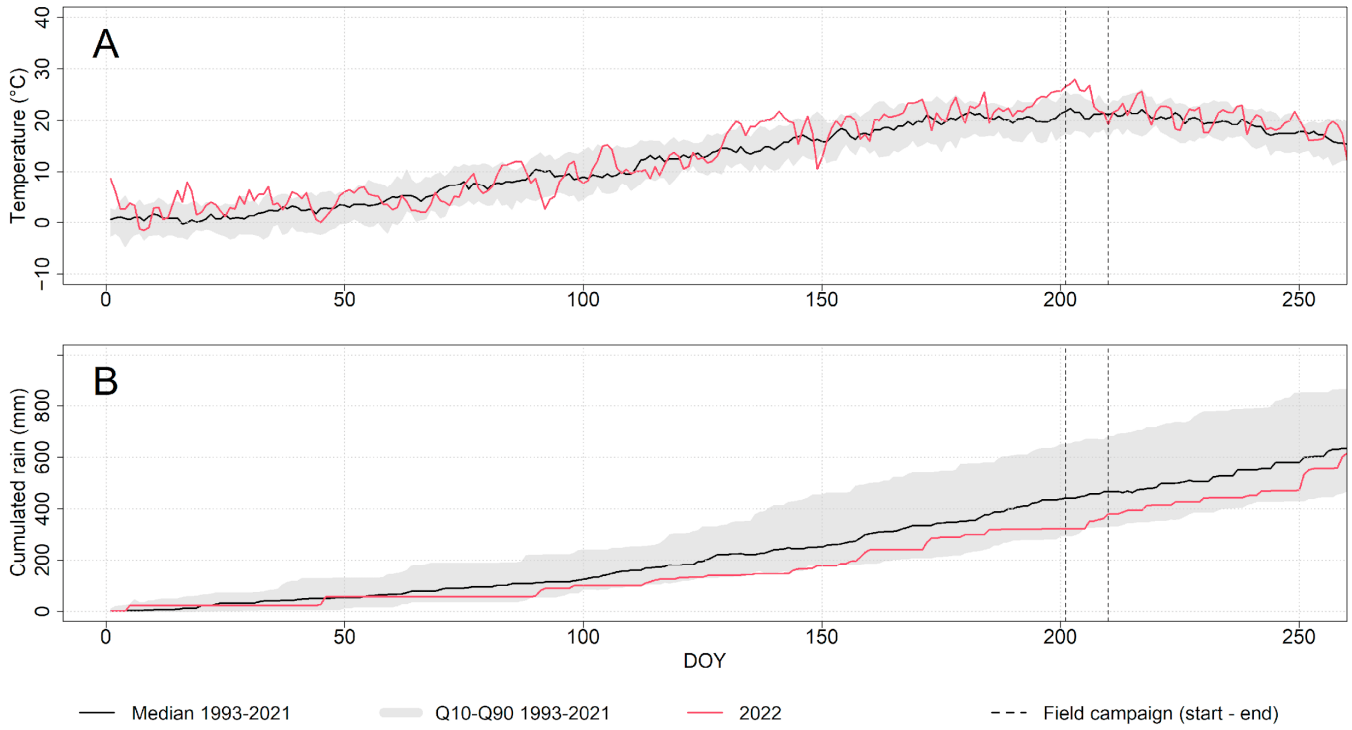

Figure 2. (**A**) Mean daily temperature of 2022 (red line), the median (black line) and the 25th and 75th percentiles (grey area) of the daily temperature for the period 1993–2021. (**B**) Cumulative precipitation in 2022 (red line) with the median (black line) and the 25th percentile and 75th percentile (grey area) of the daily rainfall for the period 1993–2021. The vertical dashed lines indicate the field campaign period.

2.3. In Situ and In-Laboratory Physiological, Biochemical and Spectral Measurements at the Leaf Level

2.3.1. Gas Exchange Measurements

Leaf gas exchange, i.e., net photosynthesis (An), stomatal conductance (gs) and transpiration rate (Tr), was measured using two portable infrared gas analyser (IRGA)-based photosynthesis systems: the LI-6400XT equipped with a fluorometer (LI-COR Biogeosciences, Lincoln, NE, USA) and the CIRAS-2 (PPSystems, Amesbury, MA, USA). The IRGA zero values (CO_2 and H_2O) of the LI-6400XT were calibrated daily, before data acquisition, using a certified N_2 tank. We set up both systems with the same settings: CO_2 concentration inside the measuring chamber (sample cell CO_2 target) at 400 ppm, leaf temperature at 28 °C (target temperature), and relative humidity between 40 and 70%. We conducted an initial test to verify that the two IRGA systems were recording consistent physiological parameter values before the field campaign.

We used the LI-6400XT system to measure photosynthesis light-response curves, adjusting PAR to the following levels: 2000, 1500, 1000, 500, 100, 50, and 0 µmol m^{-2} s^{-1}. At the end of each light-response curve, we turned off the actinic light in the chamber and left the leaf to dark-adapt for at least 30 min. At the end of the dark-acclimation period, we averaged five dark respiration rate (Rd) measurements (µmol CO_2 m^{-2} s^{-1}) taken at intervals of a few seconds. The light-response curves also included the measurement of the pulse-amplitude-modulated (PAM) chlorophyll fluorescence of light (maximum fluorescence yield in light-adapted state—Fm′, and steady-state fluorescence level in light-adapted state—Fs) and dark-adapted leaves (maximum fluorescence yield in dark-adapted state—Fm, and minimum fluorescence yield in dark-adapted state—Fo), allowing the estimation of key parameters, such as PSII operating efficiency, represented by the actual quantum yield (PhiPSII), and non-photochemical quenching (NPQ).

We used the CIRAS-2 system for more rapid determination of the leaf gas exchange, i.e., net photosynthesis at a saturating PAR of 1800 μmol m^{-2} s^{-1} (Asat), stomatal conductance, transpiration rate, and leaf temperature (Tleaf).

We measured physiological parameters on fully expanded sun-exposed leaves from the upper parts of the investigated trees.

The measurements were carried out on 22 and 24 July 2022 on the control and stressed trees and on 29 July 2022 on the irrigated tree under sunny conditions between 10:00 a.m. and 3:30 p.m.

2.3.2. Chlorophyll Content Measurements

Non-destructive measurements of leaf chlorophyll content (through the chlorophyll index—CHI) were carried out using the DUALEX optical leaf clip meter (Force-A, Orsay, France). We measured sun-exposed leaves from the upper crown of each investigated tree. We averaged the measurements on both the upper and lower sides of the leaf to obtain a single value for the leaf.

During the field campaign, leaf samples were collected from each of the investigated trees and transported to the laboratory in sealed plastic bags and stored in an ice-filled portable fridge. In the laboratory, we stored the samples at −80 °C until further processing. We extracted chlorophyll using an 80:20 v/v cold acetone:water mixture and quantified it by UV–VIS spectroscopy on a BioTek Synergy plate reader (Agilent Technologies, Inc., Santa Clara, CA, USA), following the procedure described by [38].

2.4. Remotely Sensed Data

2.4.1. LiDAR Data Acquisition and Processing

To enable tree crown segmentation of the hyperspectral image, on 26 July 2022, LiDAR data were acquired with a LiDAR miniVUX sensor (RIEGL GmbH, Horn, Austria) mounted on a DJI Matrice 600 UAV (SZ DJI Technology Co., Ltd., Shenzhen, China). A total of 42 flight lines were required to survey the 4 ha forest area, with the drone flying at an altitude of 90 m, at a speed of 6–8 m/s, and covering the area in about 72 min. LiDAR data were processed using LAStools (https://rapidlasso.de/, accessed on 10 December 2022) (rapidlasso GmbH, Gilching, Germany) to generate digital-surface and -terrain models and normalised point clouds. Tree crown segmentation for selected trees (CO1, CO2, ST1, and IR1) involved creating crown-radius buffers in QGIS (3.28.0 "Firenze") (QGIS Development Team, OSGeo, Beaverton, OR, USA) based on the mean tree crown radius measured in the field, clipping the normalised point cloud with LAStools, manually cleaning the point cloud in CloudCompare (v2.12) (CloudCompare, https://www.cloudcompare.org, accessed on 10 December 2022), and converting it to vector shapefiles. We used the obtained shapefiles to define the regions of interest (ROIs) for hyperspectral analysis (see Section 2.4.2).

2.4.2. Hyperspectral Data Acquisition and Processing

Airborne hyperspectral data were collected between 07:44:36 and 07:53:25 UTC on 26 July 2022, at an altitude of 667 m above ground level, using the AisaFENIX camera (Specim, Spectral Imaging Ltd., Oulu, Finland) with a spatial resolution of 1 m. The generated scene comprised 345 bands spanning the visible and near-infrared (VNIR, 380–970 nm) to the SWIR (970–2500 nm) spectral ranges, with a spectral resolution of ~6 nm. The acquired data were radiometrically, geometrically and atmospherically corrected using the CaliGeo (Specim, Spectral Imaging Ltd., Oulu, Finland) and the ATCOR (ReSe Applications LLC, Wil, Switzerland) software. We applied a spectral polishing filter of the neighbour-derivative type to eliminate potential artefacts by comparing the central band's value to those of the four adjacent bands, with a polishing factor of 2 on a scale from 1 to 4.

We conducted a quantitative analysis to validate the reflectance values by placing two tarps on the ground and quantifying their reflectance in absolute terms.

We used the shapefiles generated from the LiDAR data processing to ROIs for each tree crown (see Section 2.4.1). We reduced the original ROIs by excluding edge pixels to ensure the ROIs represented only the central part of the treetops, thereby eliminating border effects. We extracted reflectance values for each tree using ENVI (v5.4) (NV5 Geospatial Inc., Broomfield, CO, USA). Subsequently, we resampled the data to a 1 nm resolution. We computed key vegetation indices sensitive to (i) greenness, i.e., the NDVI, RENDVI, and CIRE, (ii) changes in xanthophyll pigments, i.e., the scaled photochemical reflectance index (SPRI), and (iii) water content, i.e., the normalised difference water index (NDWI) and NWI, using the equations reported in Table 2.

Table 2. Vegetation indices computed from the airborne hyperspectral images.

Vegetation Index	Equation	Reference
Normalised Difference Vegetation Index	$NDVI = \frac{R783-R665}{R783+R665}$	[39]
Red-Edge Normalised Difference Vegetation Index	$RENDVI = \frac{R783-R705}{R783+R705}$	[40]
Chlorophyll Index—Red-Edge	$CIRE = \frac{R740-R705}{R740+R705}$	[41]
Scaled Photochemical Reflectance Index	$SPRI = \frac{(PRI+1)}{2}$ where $PRI = \frac{R531-R570}{R531+R570}$	[42,43]
Normalised Difference Water Index	$NDWI = \frac{R865-R1240}{R865+R1240}$	[44]
Normalised Water Index	$NWI = \frac{R970-R865}{R970+R865}$	[45]

2.5. Data Analysis

As explained in Section 2.1, the experimental unit for treatment effect is the tree. Because treatment replication was lacking for the ST and IR trees (n = 1 for each treatment), formal statistical inference was not possible. Physiological measurements were conducted on different days with varying meteorological conditions (see Section 2.2). Therefore, while we present descriptive patterns (means ± SD) of leaf-level parameters pooled across treatments, these comparisons should be interpreted with caution, given both treatment effects and potential environmental confounding. These comparisons are intended to characterise observed patterns among the intensively monitored individuals and should be interpreted in light of the exploratory nature of this study. We used the R software [46] for data analysis.

3. Results

3.1. Effect of Water Stress on European Beech Physiological and Biochemical Parameters

Figure 3A reports the mean net photosynthetic light-response curve (An/PAR) for leaves of beech trees across different treatments. An showed a typical saturation trend with increasing PAR levels across all the treatments. The leaves of the irrigated tree showed the highest An values across all the PAR levels, while those of the stressed tree showed notably lower An values. Intermediate values were recorded in the CO treatment. In more detail, irrigation increased the maximum photosynthesis rate (Amax) by ~32% compared with the control, while water-stress manipulation reduced Amax by ~70% compared with the control. Moreover, the water-stress leaves showed reduced light-use efficiency (apparent quantum yield—initial slope of light-response curve), as well as reduced dark respiration rates (mean Rd of −2.09, −2.25, −1.39 μmol CO_2 m^{-2} s^{-1} for IR, CO and ST leaves, respectively).

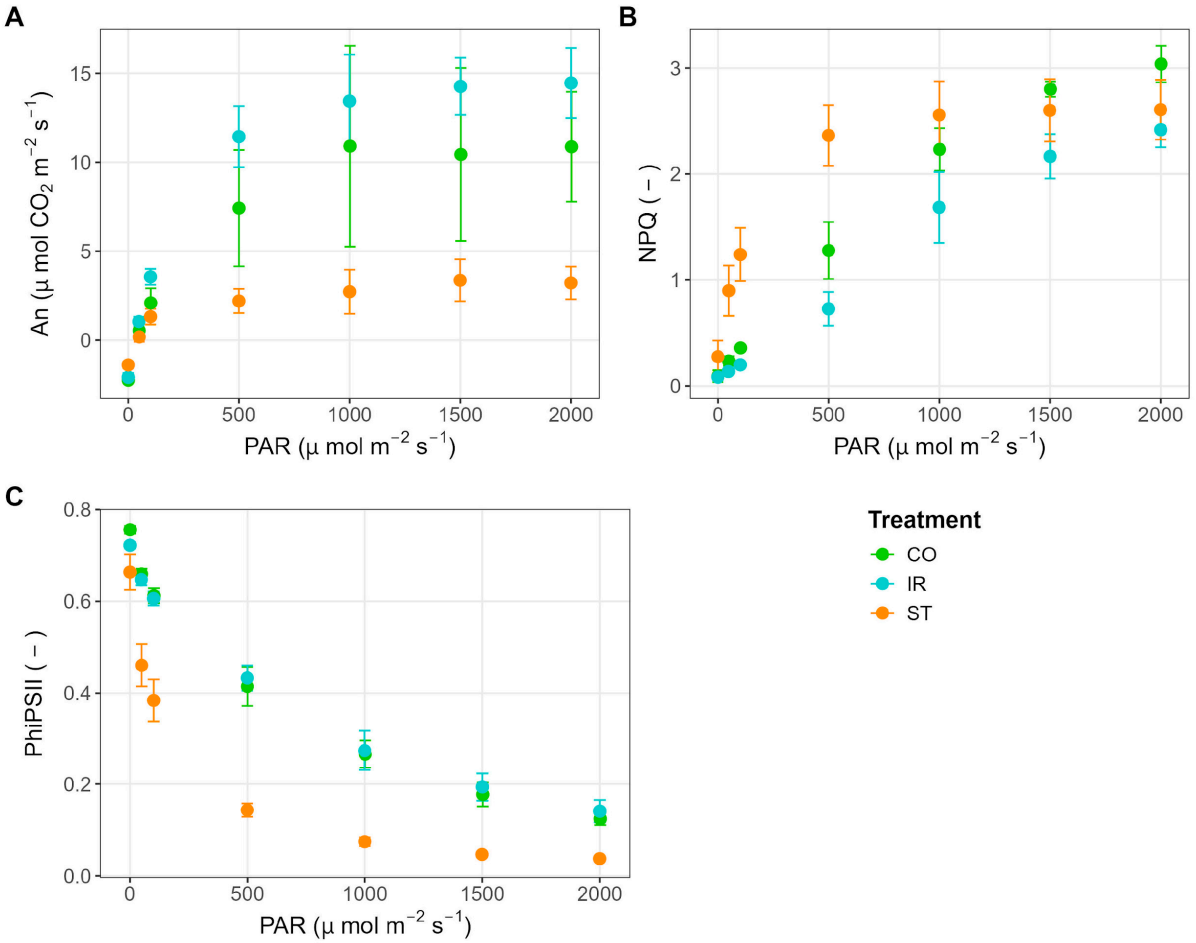

Figure 3. (**A**) Light (photosynthetically active radiation—PAR) response curves of net assimilation rate—An, (**B**) non-photochemical quenching—NPQ and (**C**) photosystem II efficiency—PhiPSII for the tree treatments. Each point represents the mean ± standard deviation. CO, IR and ST refer to leaves of control (n = 2), irrigated (n = 3) and water-stressed (n = 3) trees, respectively.

In Figure 3B, the trend of the mean NPQ, representing the dissipation of excess light energy as heat, is shown for leaves of trees under the three treatments. NPQ increased with increasing PAR in all the treatments, indicating enhanced photoprotective heat dissipation at high light levels. The leaves of the stressed tree exhibited higher NPQ values than those of the other treatments until intermediate PAR levels (up to 1000 μmol m^{-2} s^{-1}). At higher PAR levels, the NPQ in the ST leaves showed a clear saturating trend and consequently remained closer to the values of the other treatments.

Figure 3C shows that the actual quantum yield of PSII decreased with increasing PAR. The leaves of the irrigated and control trees maintained high photosystem II efficiency. In contrast, the leaves of the stressed tree showed lower PSII efficiency, dropping sharply even at low PAR levels.

Also, gas exchange measurements under saturating PAR levels, performed on a larger number of leaves, revealed that the Tr, Asat, and gs values differed across the three treatments (Table 3). The leaves of the stressed tree showed the lowest values of Tr, Asat, and gs, whereas the leaves of the irrigated tree showed the highest values of photosynthetic rate and associated parameters. In fact, the mean Asat value for the irrigated tree was 18.14 μmol CO_2 m^{-2} s^{-1}, which was distinctly higher than the mean for the control trees (12.24 μmol CO_2 m^{-2} s^{-1}) and the stressed tree (4.99 μmol CO_2 m^{-2} s^{-1}).

Table 3. Leaf gas exchange values (mean ± standard deviation) measured during Asat determination on 13 CO leaves, 8 IR leaves and 14 ST leaves.

	Treatment		
	CO	**IR**	**ST**
Tr (mmol H_2O m^{-2} s^{-1})	4.79 ± 1.01	8.19 ± 0.693	2.99 ± 0.63
Asat (µmol CO_2 m^{-2} s^{-1})	12.24 ± 3.39	18.14 ± 3.07	4.99 ± 2.34
gs (mmol m^{-2} s^{-1})	250.54 ± 63.39	532.63 ± 71.30	132.0 ± 33.63
Tleaf (°C)	28.45 ± 0.88	29.04 ± 1.18	28.54 ± 0.97

The mean values of the chlorophyll index (CHI) obtained with the DUALEX leaf clip, and the total chlorophyll content (chlorophyll a + chlorophyll b, Total Chl) determined through UV–VIS spectroscopy, are reported in Table 4. The CHI values were lower in the water-stressed trees (27.79 ± 4.28) than in the control (37.48 ± 5.87) and irrigated trees (39.05 ± 2.73), indicating reduced chlorophyll content under experimentally induced drought conditions.

Table 4. Mean values ± standard deviation of (i) the chlorophyll index (CHI) measured using the DUALEX clip in 74 CO leaves, 30 IR leaves and 45 ST leaves, and (ii) the total chlorophyll content (chlorophyll a + chlorophyll b, Total Chl) determined by UV–VIS spectroscopic laboratory method in 43 CO leaves, 15 IR leaves and 28 ST leaves.

	Treatment		
	CO	**IR**	**ST**
CHI	37.48 ± 5.87	39.05 ± 2.73	27.79 ± 4.28
Total Chl (mg/g)	5.98 ± 1.06	5.84 ± 0.87	3.86 ± 0.94

The results from the independent laboratory method confirmed this behaviour. The leaves of the control and irrigated trees showed very similar total chlorophyll content (Total Chl), with mean values of 5.98 mg/g and 5.84 mg/g, respectively. By comparison, the leaves of the water-stressed tree contained approximately 35% less total chlorophyll content than those of the control and irrigated trees (3.86 ± 0.94 mg/g).

3.2. Effect of Water Stress on European Beech Crown Reflectance and Spectral Vegetation Indices

Figure 4 shows the mean hyperspectral reflectance at the crown level from airborne data. The reflectance of the crown for the ST treatment was slightly higher in the visible domain, while the IR crown response appears evident for the typical water features in the NIR and SWIR spectral domains.

Figure 5 shows the trend of the hyperspectral reflectance indices computed at the crown level from the airborne hyperspectral data. The NDVI did not differ markedly among tree crowns across the three treatments. On the other hand, the chlorophyll vegetation indices, including the RENDVI and CIRE, showed distinct values across the CO, IR, and ST treatments. For both chlorophyll indices, the highest values were observed in the crown of the irrigated tree, while the lowest values were recorded in the crown of the ST tree. Intermediate values characterised the CO treatment. The SPRI followed a pattern similar to that of the chlorophyll indices. By comparison, the water-related vegetation indices did not reveal a clear pattern of leaf water status across the analysed trees. In more detail, although the water-index values were higher in the IR tree than in the other treatments, they did not differ notably between the CO and ST trees.

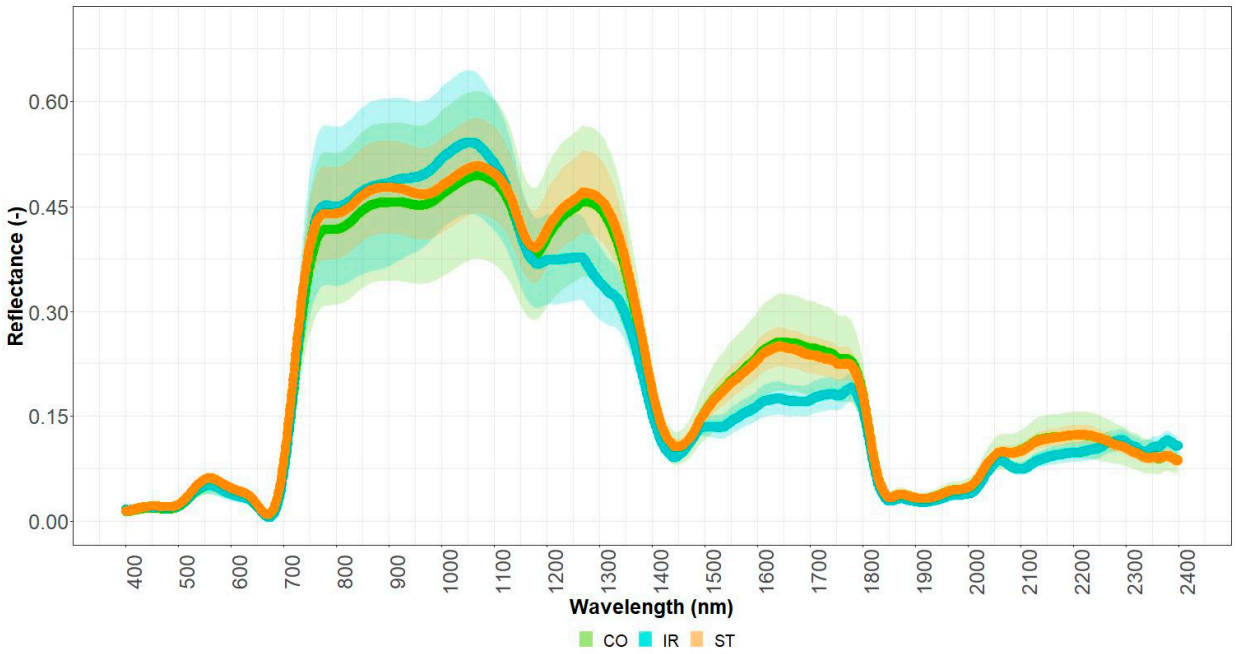

Figure 4. Mean hyperspectral reflectance at the crown level from airborne data for each treatment: control (CO), irrigation (IR), and water stress (ST).

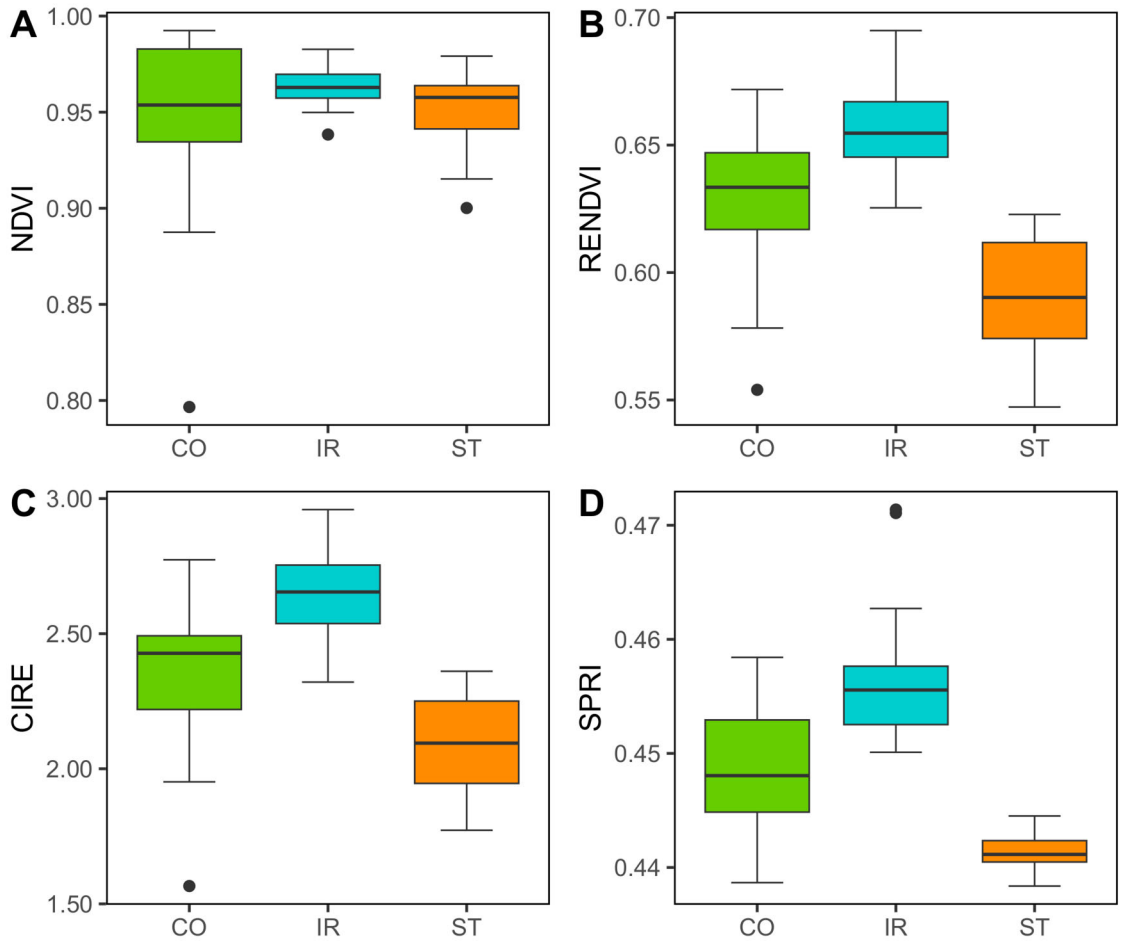

Figure 5. *Cont.*

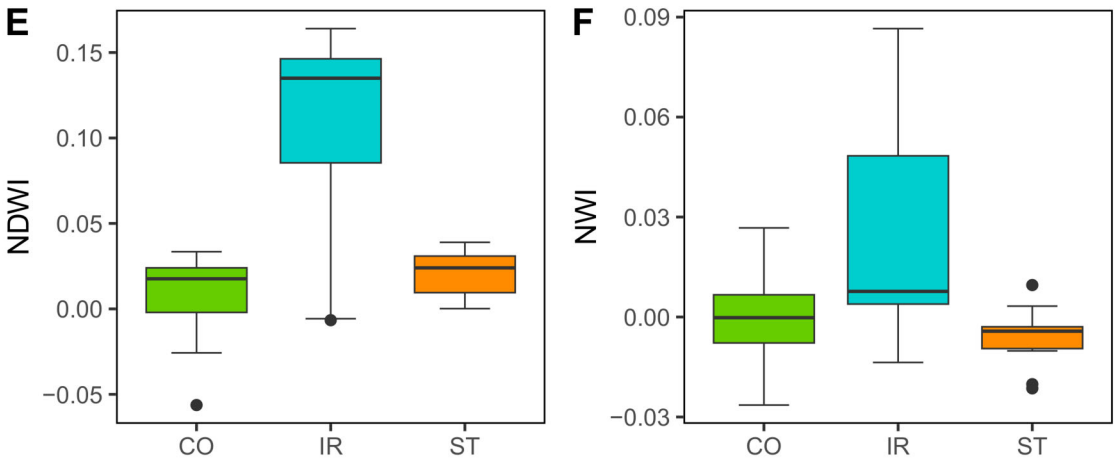

Figure 5. NDVI (**A**), RENDVI (**B**), CIRE (**C**), SPRI (**D**), NDWI (**E**), and NWI (**F**) calculated from crown-level hyperspectral reflectance obtained from airborne data for the three treatments: control (CO), irrigated (IR), and water-stressed (ST). Box plots show the interquartile range (IQR), with the horizontal line in the box indicating the median. Whiskers extend to the minimum and maximum values, excluding outliers, which are shown as individual points.

4. Discussion

4.1. Effect of the CDHW Event and the Manipulation-Induced Water Stress on European Beech Physiological and Biochemical Parameters

This exploratory study investigated the physiological and spectral responses of individual European beech trees experiencing different water-availability conditions during the 2022 CDHW event. While the limited sample size precludes definitive conclusions about species-level responses, our intensive measurements on four trees provide detailed insights into physiological–spectral relationships.

Our results show that the trees under the three treatments exhibited distinct physiological signatures. The leaves of the irrigated tree displayed the highest photosynthetic rates across the entire PAR range, accompanied by the lowest NPQ values, indicating highly efficient photochemistry. The leaves of the control trees showed intermediate photosynthesis and the highest peak NPQ values, suggesting moderate stress and a greater reliance on regulated thermal dissipation. Although the NPQ of both the CO and IR leaves increased with increasing PAR, which indicated that the trees' ability to dissipate excess light energy through NPQ was maintained in the CO leaves during the CDHW event, the higher NPQ values, together with the lower photosynthesis rates observed in the CO leaves compared to the IR leaves, suggest that the CO leaves were experiencing mild physiological stress, resulting in higher excess excitation energy and more substantial photoprotective heat dissipation.

The leaves of the ST tree showed severely suppressed photosynthesis and a clear NPQ saturation plateau, consistent with other studies of plant stress [47,48]. In our research, the NPQ in the ST tree appeared to saturate at PAR levels below 1000 µmol m^{-2} s^{-1}. Moreover, the NPQ values of the ST leaves remained elevated even at low PAR levels, and dark NPQ was substantially higher than in the other treatments, indicating chronic stress, sustained energy dissipation, photoinhibition of PSII, and an increased risk of oxidative stress. Together, these patterns reveal that water stress severely limits CO_2 utilisation, forcing maximal use of photoprotective NPQ, whereas irrigation maintains high photochemical efficiency with minimal dissipation demand.

The CDHW stress experienced by the CO trees was associated with lower photosynthetic capacity and higher NPQ than in the IR tree. However, it did not reduce chlorophyll content (estimated in situ and measured in the laboratory), indicating that the reduced

photosynthesis in the CO trees was primarily driven by functional limitations (e.g., stomatal and biochemical limitations) rather than pigment differences. At the same time, the chlorophyll content was significantly lower in the leaves of the ST tree, most likely due to the inactivation of chlorophyll biosynthesis enzymes, oxidative damage to chloroplast lipids, or chlorophyll degradation [49]. Consequently, photosynthesis in the leaves of the ST tree was dramatically reduced compared to that in the leaves of the CO or IR trees as a result of both structural and functional limitations. The results from our drought-manipulation experiment suggest that more pronounced or prolonged stress under future climate scenarios might influence pigment pools and trigger additional photosynthetic impairments in European beech, as also indicated by [50].

4.2. Traceability of Drought Stress Through Hyperspectral Indices Measured at the Tree-Crown Level

Among the hyperspectral indices derived from the airborne data, the NDVI failed to detect differences in greenness across the different treatments. This result could be explained by the well-known fact that the NDVI is less sensitive to slight changes in chlorophyll content, especially at full canopy cover [51,52]. On the other hand, chlorophyll-sensitive indices, such as the RENDVI, have demonstrated to be much more sensitive to stress-induced changes. However, given that the measured leaf chlorophyll content was comparable between the CO and IR treatments and significantly lower in the ST treatment, only the RENDVI differences between ST and CO were likely driven by differences in total leaf chlorophyll content. Conversely, the differences regarding the RENDVI between the CO and IR trees could suggest minor variations in canopy structure and architecture induced by the sub-optimal water status of the CO tree during the CDHW event. Architectural plant traits, as demonstrated in the literature, have been shown to cause significant canopy spectral responses [25]. Similar results emerged for another chlorophyll index, the CIRE: it showed very low values in stressed trees, much higher values in control trees exposed to the 2022 CDHW event, and the highest values in the IR treatment, which received supplemental water. This outcome potentially suggests that both changes in chlorophyll content and slight modifications in crown architecture may have occurred across the treatments. In particular, architectural changes might have played a significant role during the CDHW event. In this context, previous studies [53] observed that adult trees can modify leaf angle distribution to reduce exposure to excessive radiation, thereby limiting photosynthetic capacity.

The water-related vegetation indices showed higher values for the IR treatment, whereas the water indices for the CO and ST treatments did not differ markedly. The lack of clear differentiation between the CO and ST trees regarding the water indices may indicate that: (i) the bulk canopy water content in the ST tree may not have been substantially depleted despite pronounced reductions in leaf-level photosynthesis and chlorophyll content; and/or (ii) the canopy-scale water indices may have been confounded by canopy structural effects or background contributions in the 1 m spatial resolution imagery, further limiting their ability to detect subtle differences. More detailed studies are needed to determine the effectiveness of SWIR-based indices in characterising single-tree spectral responses to stress, including CDHW events [54].

The SPRI showed that structural integrity and pigment status were compromised at the crown level in the stressed European beech tree but remained intact under irrigation, with the stressed tree exhibiting the lowest SPRI values.

A recent study on the impact of the 2022 CDHW in the same geographical area, investigating forests across different altitudes and forest types [55], observed two contrasting behaviours: the canopy greenness of tree species located at a median altitude above 1000 m a.s.l. generally increased, while the canopy greenness of tree species below 1000 m a.s.l. was

typically negatively impacted. In European beech forests, Ref. [55] observed contrasting impacts across altitudes and locations. Our study indicates that, although drought-related impacts on NDVI values were absent at the Cembra site, chlorophyll indices such as the RENDVI and CIRE have the potential to track differences among treatments.

In a changing climate, remote sensing can be used to retrieve key proxies, such as chlorophyll indices, the PRI, water indices and solar-induced Chl fluorescence (SIF), to improve stress detection and upscale observations [56]. In particular, the combination of hyperspectral images and SIF may prove particularly useful for detecting physiological stress that does not cause significant changes in pigment content [47], as observed in the CO treatment in our study. Airborne hyperspectral data proved to be suitable for detecting drought stress in European beech. They can be considered a key tool in the current efforts to build a pan-European monitoring and evaluation framework, such as the FORWARDS initiative (https://forwards-project.eu/, accessed on 5 December 2025), which will help to demonstrate the impact of climate change on forests.

In Europe, several cases of forest degradation are occurring [57]. Severe oak decline is evident and affects different *Quercus* spp. across a wide range of ecosystems and bioclimatic regions, from Mediterranean areas to Central Europe [58]. At the same time, stress in *Pinus* spp. forests has been documented and is raising increasing concerns [59]. Although the current status of European beech does not raise major concerns, significant stress symptoms are already evident in Central Europe [60]. According to climate projections, a relevant area of the current European beech stands may fall outside their bioclimatic niche by the middle of this century [61]; therefore, accurate remote sensing observations will be needed to monitor forest stands' health status and guide proper management strategies to maintain both structural diversity [62] and species diversity [63].

4.3. Study Limitations and Future Research Priorities

Despite enabling intensive physiological and spectral characterisation, our exploratory approach presents limitations that should guide interpretation and future research.

The logistical complexity and labour-intensive nature of the field campaign constrained the experimental approach of this study. Reaching the upper sunlit canopy of mature beech trees at heights up to 20 m required specialised mobile elevating work platforms (Figure 1), which significantly limited the number of trees that could be intensively monitored during the brief measurement window coinciding with the 2022 CDHW event. Consequently, the limited number of trees investigated precludes robust statistical inference about treatment effects relative to individual-tree variability. The observed physiological and spectral differences may reflect not only water status but also microsite differences in soil characteristics, variations in the competitive environment, or pre-existing differences in tree vigour.

An additional limitation concerns pseudo-replication arising from the experimental design. Although a large number of leaf-level physiological measurements and crown-level hyperspectral pixels were collected, these observations are nested within a very limited number of individual trees. As a result, as already explained, leaves and pixels cannot be considered independent experimental units, and the effective sample size for treatment comparisons corresponds to the number of trees per treatment (n = 1–2). This pseudo-replication has important statistical consequences. First, it may inflate the apparent strength and significance of treatment effects by underestimating uncertainty and increasing the risk of Type I errors. Second, it prevents robust separation of treatment effects from individual-tree idiosyncrasies, such as microsite conditions, rooting patterns, or pre-existing physiological status. Therefore, the observed differences among the treatments should be interpreted as contrasts among intensively monitored individuals rather than as

population-level responses of European beech. For these reasons, we did not apply statistical analyses; instead, we adopted a descriptive and exploratory approach to characterise the internal consistency and magnitude of physiological and spectral responses within individual trees rather than to provide confirmatory inference on treatment effects. The coherence observed between leaf-level physiology and crown-level hyperspectral indices supports the mechanistic plausibility of the detected patterns but does not imply generality beyond the studied individuals. In the context of remote sensing, pseudo-replication at the pixel level may further exaggerate confidence in spectral separability among treatments as numerous spatial observations originate from the same crown. The validation of hyperspectral drought indices therefore requires replication across multiple trees, stands, and environmental conditions to ensure transferability and operational robustness. Despite this constraint, the intensive high-resolution monitoring of each tree provided valuable insights into physiological responses to contrasting water regimes and a foundation for designing future studies, which should include proper replication, involving multiple trees per treatment across representative site conditions.

Finally, the timing of irrigation relative to the hyperspectral acquisition might have introduced additional uncertainty. Overall, while our results indicate that irrigation effectively increased both leaf physiological activity and canopy water content, some nonlinearity in canopy water content immediately after irrigation cannot be entirely ruled out. We acknowledge this as a limitation and note that high-frequency physiological and remote sensing measurements following controlled irrigation events would be valuable in future studies to capture these potential dynamics.

Nevertheless, despite these limitations, this exploratory study demonstrates the feasibility of combining intensive physiological monitoring with hyperspectral remote sensing to detect stress in individual trees. The methodology provides a foundation for future research, with proper replication, adequate controls, and multi-year monitoring, to definitively characterise European beech drought responses and to validate operational remote sensing approaches for forest monitoring under climate change.

As the frequency and intensity of CDHW events are expected to increase under future climate scenarios, detailed investigations of spatial and temporal drought responses are needed to guide forest practitioners in implementing appropriate management strategies [64].

The priority areas for future research include: (1) replicated experiments with appropriate infrastructure (towers and mobile platforms) across multiple sites spanning the species' climatic range; (2) continuous monitoring of soil moisture, sap flow, and stem growth to track the development and evolution of stress; (3) multi-year observations to capture inter-annual climate variability; (4) mechanistic studies linking leaf-level optical properties to canopy-scale spectral signatures; (5) validation of remote sensing indices against physiological stress metrics across diverse forest conditions; and (6) integration with process-based models to predict drought impacts under future climate scenarios.

5. Conclusions

This exploratory study combined intensive physiological monitoring with airborne hyperspectral remote sensing to investigate the drought-stress sensitivity and stress detectability in a European beech stand in the eastern Alps of Italy during the 2022 CDHW event. Our physiological measurements revealed that the water-stressed beech tree exposed to the manipulation experiment exhibited severely reduced photosynthetic capacity, accompanied by substantial chlorophyll degradation. In contrast, trees under ambient 2022 CDHW conditions showed mild photosynthetic impairment without chlorophyll loss,

suggesting that early-stage stress affects beech trees' stomatal and metabolic functions before detectable pigment changes occur.

This pilot study suggests that red-edge vegetation indices (RENDVI and CIRE) and photochemical reflectance indices (SPRI) can differentiate trees with varying photosynthetic status and hold promise for operational stress detection. Water-related vegetation indices showed higher values for the IR treatment; however, further studies are needed to investigate the spectral responses of water-absorption-related features to subtle changes in canopy water status.

The intensive measurement approach demonstrated here, while logistically challenging, provides critical ground-truth data for validating satellite remote sensing products. Many of the investigated indices yield scale-appropriate pixels for forest monitoring at either the single-tree (PlanetScope) or plot level (Sentinel-2, PRISMA). The methodological framework and the demonstrated feasibility of this approach are the key outcomes of this pilot study, paving the way for future replicated studies.

Author Contributions: Conceptualisation, K.S. and C.T.; methodology, K.S. and C.T.; software, K.S., M.E., M.R. and C.T.; validation, K.S., C.T. and L.V.; formal analysis, K.S. and C.T.; investigation, K.S., M.R., F.U., S.P., L.V. and C.T.; resources, K.S., L.B.M., M.D., M.E., M.R., F.U., S.P., L.V. and C.T.; data curation, K.S., M.D., M.E., M.R., F.U. and S.P.; writing—original draft preparation, C.T.; writing—review and editing, K.S., L.B.M., M.D., M.E., M.R., F.U., S.P., L.V., L.A.C. and C.T.; visualisation, K.S. and C.T.; supervision, K.S., C.T. and L.V.; project administration, C.T. and K.S.; funding acquisition, C.T. All authors have read and agreed to the published version of the manuscript.

Funding: This research was carried out within the FaguSense project, funded by the Department of Biology, Agriculture and Food Science of the National Research Council of Italy, through the 2021 "Call for access to the National Research infrastructures of the Italian Plant Phenotyping network Phen-Italy" (grant number 0052098/2021).

Data Availability Statement: The raw data supporting the conclusions of this article will be made available by the authors on request.

Acknowledgments: We are grateful to Mauro Cavagna, Isaac Chini, Lorenzo Frizzera, and Roberto Zampedri of the Edmund Mach Foundation, and to Silvia Baronti of the National Research Council of Italy for their support during and after the field campaign.

Conflicts of Interest: The authors declare no conflicts of interest. The funders had no role in the design of the study, the collection, analysis, or interpretation of data, the writing of the manuscript, or the decision to publish the results.

Abbreviations

The following abbreviations are used in this manuscript:

Amax	maximum photosynthesis rate
An	net photosynthesis
Asat	net photosynthesis at a saturating PAR
CDHW	compound drought and heatwave
CHI	chlorophyll index
CIRE	chlorophyll red-edge index
ETR	electron transport rate
Fm	maximum fluorescence yield in the dark-adapted state
Fm′	maximum fluorescence yield in the light-adapted state
Fo	minimum fluorescence yield in dark-adapted state
Fs	steady-state fluorescence level in the light-adapted state
Fv/Fm	maximum potential quantum efficiency of photosystem II
gs	stomatal conductance
IRGA	infrared gas analyser

LAI	leaf area index
NDVI	normalised difference vegetation index
NDWI	normalised difference water index
NIR	near-infrared
NPQ	non-photochemical quenching
NWI	normalised water index
PAM	pulse-amplitude-modulated
PAR	photosynthetically active radiation
PRI	photochemical reflectance index
PSII	photosystem II
Rd	dark respiration rate
RENDVI	red-edge normalised difference vegetation index
ROI	region of interest
SPRI	scaled photochemical reflectance index
SVI	spectral vegetation index
SWIR	shortwave infrared
Tr	transpiration rate
VIS	visible
VNIR	visible and near-infrared

References

1. Beniston, M. Extreme climatic events: Examples from the alpine region. *J. De Phys. IV* **2004**, *121*, 139–149. [CrossRef]
2. Reichstein, M.; Bahn, M.; Ciais, P.; Frank, D.; Mahecha, M.D.; Seneviratne, S.I.; Zscheischler, J.; Beer, C.; Buchmann, N.; Frank, D.C.; et al. Climate extremes and the carbon cycle. *Nature* **2013**, *500*, 287–295. [CrossRef] [PubMed]
3. Zwiers, F.W.; Alexander, L.V.; Hegerl, G.C.; Knutson, T.R.; Kossin, J.P.; Naveau, P.; Nicholls, N.; Schär, C.; Seneviratne, S.I.; Zhang, X. Climate Extremes: Challenges in Estimating and Understanding Recent Changes in the Frequency and Intensity of Extreme Climate and Weather Events. In *Climate Science for Serving Society*; Asrar, G., Hurrell, J., Eds.; Springer: Dordrecht, The Netherlands, 2013. [CrossRef]
4. Perkins, S.E.; Alexander, L.V. On the measurement of heat waves. *J. Clim.* **2013**, *26*, 4500–4517. [CrossRef]
5. Van Loon, A.F. Hydrological drought explained. *Wiley Interdiscip. Rev. Water* **2015**, *2*, 359–392. [CrossRef]
6. Zhang, Q.; She, D.; Zhang, L.; Wang, G.; Chen, J.; Hao, Z. High Sensitivity of Compound Drought and Heatwave Events to Global Warming in the Future. *Earth's Future* **2022**, *10*, e2022EF002833. [CrossRef]
7. Peel, M.C.; Finlayson, B.L.; Mcmahon, T.A. Hydrology and Earth System Sciences Updated world map of the Köppen-Geiger climate classification. *Hydrol. Earth Syst. Sci.* **2007**, *11*, 1633–1644. [CrossRef]
8. Stephan, R.; Erfurt, M.; Terzi, S.; Zun, M.; Kristan, B.; Haslinger, K.; Stahl, K. An inventory of Alpine drought impact reports to explore past droughts in a mountain region. *Nat. Hazards Earth Syst. Sci.* **2021**, *21*, 2485–2501. [CrossRef]
9. Calanca, P. Climate change and drought occurrence in the Alpine region: How severe are becoming the extremes? *Glob. Planet. Change* **2007**, *57*, 151–160. [CrossRef]
10. Beniston, M.; Stephenson, D.B. Extreme climatic events and their evolution under changing climatic conditions. *Glob. Planet. Change* **2004**, *44*, 1–9. [CrossRef]
11. Lhotka, O.; Kyselý, J. The 2021 European Heat Wave in the Context of Past Major Heat Waves. *Earth Space Sci.* **2022**, *9*, e2022EA002567. [CrossRef]
12. EEA. European forest types. In *Categories and Types for Sustainable Forest Management Reporting and Policy*; EEA Technical Report No 9/2006; Office for Official Publications of the European Communities: Luxembourg, 2006; ISSN 1725-2237. Available online: https://foresteurope.org/wp-content/uploads/2022/01/WFC_4_eea_technical_report_92006.pdf (accessed on 5 December 2025).
13. Oddi, L.; Migliavacca, M.; Cremonese, E.; Filippa, G.; Vacchiano, G.; Siniscalco, C.; Morra Di Cella, U.; Galvagno, M. Contrasting responses of forest growth and carbon sequestration to heat and drought in the Alps. *Environ. Res. Lett.* **2022**, *17*, 045015. [CrossRef]
14. Páscoa, P.; Gouveia, C.M.; Russo, A.C.; Bojariu, R.; Vicente-Serrano, S.M.; Trigo, R.M. Vegetation vulnerability to drought on southeastern Europe. *Hydrol. Earth Syst. Sci. Discuss.* **2018**, *2018*, 1–29. [CrossRef]
15. Bussotti, F.; Papitto, G.; di Martino, D.; Cocciufa, C.; Cindolo, C.; Cenni, E.; Bettini, D.; Iacopetti, G.; Ghelardini, L.; Moricca, S.; et al. Extreme climatic events, biotic interactions and species-specific responses drive tree crown defoliation and mortality in Italian forests. *IForest* **2024**, *17*, 300–308. [CrossRef]

16. Laoué, J.; Havaux, M.; Ksas, B.; Orts, J.P.; Reiter, I.M.; Fernandez, C.; Ormeno, E. A decade of rain exclusion in a Mediterranean forest reveals trade-offs of leaf chemical defenses and drought legacy effects. *Sci. Rep.* **2024**, *14*, 24119. [CrossRef]
17. Iacopetti, G.; Selvi, F.; Bussotti, F.; Pollastrini, M.; Jucker, T.; Bouriaud, O. Tree diversity and identity modulate the growth response of thermophilous deciduous forests to climate warming. *Oikos* **2023**, *2023*, e08875. [CrossRef]
18. Vanhellemont, M.; Sousa-Silva, R.; Maes, S.L.; van den Bulcke, J.; Hertzog, L.; de Groote, S.R.E.; van Acker, J.; Bonte, D.; Martel, A.; Lens, L.; et al. Distinct growth responses to drought for oak and beech in temperate mixed forests. *Sci. Total Environ.* **2019**, *650*, 3017–3026. [CrossRef]
19. Rennenberg, H.; Loreto, F.; Polle, A.; Brilli, F.; Fares, S.; Beniwal, R.S.; Gessler, A. Physiological responses of forest trees to heat and drought. *Plant Biol.* **2006**, *8*, 556–571. [CrossRef]
20. Teskey, R.; Wertin, T.; Bauweraerts, I.; Ameye, M.; McGuire, M.A.; Steppe, K. Responses of tree species to heat waves and extreme heat events. *Plant Cell Environ.* **2015**, *38*, 1699–1712. [CrossRef]
21. Putzenlechner, B.; Koal, P.; Kappas, M.; Löw, M.; Mundhenk, P.; Tischer, A.; Wernicke, J.; Koukal, T. Towards precision forestry: Drought response from remote sensing-based disturbance monitoring and fine-scale soil information in Central Europe. *Sci. Total Environ.* **2023**, *880*, 163114. [CrossRef]
22. Xu, C.; Liu, H.; Ciais, P.; Hartmann, H.; Camarero, J.J.; Wu, X.; Hammond, W.M.; Allen, C.D.; Chen, F. Enhanced Drought Exposure Increasingly Threatens More Forests Than Observed. *Earth's Future* **2024**, *12*, e2023EF003705. [CrossRef]
23. Zeng, Y.; Hao, D.; Huete, A.; Dechant, B.; Berry, J.; Chen, J.M.; Joiner, J.; Frankenberg, C.; Bond-Lamberty, B.; Ryu, Y.; et al. Optical vegetation indices for monitoring terrestrial ecosystems globally. *Nat. Rev. Earth Environ.* **2022**, *3*, 477–493. [CrossRef]
24. Rouse, J.W., Jr.; Haas, R.H.; Schell, J.A.; Deering, D.W. Monitoring the Vernal Advancement and Retrogradation (Green Wave Effect) of Natural Vegetation (No. NASA-CR-132982). 1973. Available online: https://ntrs.nasa.gov/api/citations/19730017588/downloads/19730017588.pdf (accessed on 5 December 2025).
25. Imran, H.A.; Gianelle, D.; Rocchini, D.; Dalponte, M.; Martín, M.P.; Sakowska, K.; Wohlfahrt, G.; Vescovo, L. VIS-NIR, Red-Edge and NIR-Shoulder Based Normalised Vegetation Indices Response to Co-Varying Leaf and Canopy Structural Traits in Heterogeneous Grasslands. *Remote Sens.* **2020**, *12*, 2254. [CrossRef]
26. Castro, S.; Sanchez-Azofeifa, A. Testing of automated photochemical reflectance index sensors as proxy measurements of light use efficiency in an aspen forest. *Sensors* **2018**, *18*, 3302. [CrossRef]
27. Gamon, J.A.; Wang, R.; Russo, S.E. Contrasting photoprotective responses of forest trees revealed using PRI light responses sampled with airborne imaging spectrometry. *New Phytol.* **2023**, *238*, 1318–1332. [CrossRef]
28. Nakamura, Y.; Tsujimoto, K.; Ogawa, T.; Noda, H.M.; Hikosaka, K. Correction of photochemical reflectance index (PRI) by optical indices to predict non-photochemical quenching (NPQ) across various species. *Remote Sens. Environ.* **2024**, *305*, 114062. [CrossRef]
29. Zhang, Y.; Wang, A.; Li, J.; Wu, J. Water content estimation of conifer needles using leaf-level hyperspectral data. *Front. Plant Sci.* **2024**, *15*, 1428212. [CrossRef]
30. Liu, Q.; Jia, W.; Li, F. Determination of the most effective design for the measurement of photosynthetic light-response curves for planted Larix olgensis trees. *Sci. Rep.* **2020**, *10*, 1–10. [CrossRef] [PubMed]
31. Roy, J.; Tardieu, F.; Tixier-Boichard, M.; Schurr, U. European infrastructures for sustainable agriculture. *Nat. Plants* **2017**, *3*, 756–758. [CrossRef] [PubMed]
32. Lu, R.; Xu, K.; Chen, R.; Chen, W.; Li, F.; Lv, C. Heat waves in summer 2022 and increasing concern regarding heat waves in general. *Atmos. Ocean. Sci. Lett.* **2023**, *16*, 100290. [CrossRef]
33. Tripathy, K.P.; Mishra, A.K. How Unusual Is the 2022 European Compound Drought and Heatwave Event? *Geophys. Res. Lett.* **2023**, *50*, e2023GL105453. [CrossRef]
34. Feser, F.; van Garderen, L.; Hansen, F. The Summer Heatwave 2022 over Western Europe: An Attribution to Anthropogenic Climate Change. *Bull. Am. Meteorol. Soc.* **2024**, *105*, E2175–E2179. [CrossRef]
35. Faranda, D.; Pascale, S.; Bulut, B. Persistent anticyclonic conditions and climate change exacerbated the exceptional 2022 European-Mediterranean drought. *Environ. Res. Lett.* **2023**, *18*, 034030. [CrossRef]
36. Choler, P. Above-treeline ecosystems facing drought: Lessons from the 2022 European summer heat wave. *Biogeosciences* **2023**, *20*, 4259–4272. [CrossRef]
37. Kellerer-Pirklbauer, A.; Eulenstein, J. The summer heatwave in 2022 and its role in changing permafrost and periglacial conditions at a historic mountain pass in the Eastern Alps (Hochtor, Hohe Tauern Range, Austria). *Permafr. Periglac. Process.* **2023**, *34*, 547–565. [CrossRef] [PubMed]
38. Lichtenthaler, H.K.; Buschmann, C. Chlorophylls and Carotenoids: Measurement and Characterisation by UV-VIS Spectroscopy. *Curr. Protoc. Food Anal. Chem.* **2001**, *1*, F4.3.1–F4.3.8. [CrossRef]

39. Moncholi-Estornell, A.; Cendrero-Mateo, M.P.; Antala, M.; Cogliati, S.; Moreno, J.; van Wittenberghe, S. Enhancing Solar-Induced Fluorescence Interpretation: Quantifying Fractional Sunlit Vegetation Cover Using Linear Spectral Unmixing. *Remote Sens.* **2023**, *15*, 4274. [CrossRef]
40. Evangelides, C.; Nobajas, A. Red-Edge Normalised Difference Vegetation Index (NDVI705) from Sentinel-2 imagery to assess post-fire regeneration. *Remote Sens. Appl. Soc. Environ.* **2020**, *17*, 100283. [CrossRef]
41. Zhang, H.; Li, J.; Liu, Q.; Lin, S.; Huete, A.; Liu, L.; Croft, H.; Clevers, J.G.P.W.; Zeng, Y.; Wang, X.; et al. A novel red-edge spectral index for retrieving the leaf chlorophyll content. *Methods Ecol. Evol.* **2022**, *13*, 2771–2787. [CrossRef]
42. Drolet, G.G.; Huemmrich, K.F.; Hall, F.G.; Middleton, E.M.; Black, T.A.; Barr, A.G.; Margolis, H.A. A MODIS-derived photochemical reflectance index to detect inter-annual variations in the photosynthetic light-use efficiency of a boreal deciduous forest. *Remote Sens. Environ.* **2005**, *98*, 212–224. [CrossRef]
43. Sukhova, E.; Sukhov, V. Connection of the photochemical reflectance index (PRI) with the photosystem II quantum yield and non-photochemical quenching can be dependent on variations of photosynthetic parameters among investigated plants: A meta-analysis. *Remote Sens.* **2018**, *10*, 771. [CrossRef]
44. Gao, B.-C. NDWI—A normalised difference water index for remote sensing of vegetation liquid water from space. *Remote Sens. Environ.* **1996**, *58*, 257–266. [CrossRef]
45. Babar, M.A.; Reynolds, M.P.; van Ginkel, M.; Klatt, A.R.; Raun, W.R.; Stone, M.L. Spectral reflectance indices as a potential indirect selection criteria for wheat yield under irrigation. *Crop Sci.* **2006**, *46*, 578–588. [CrossRef]
46. R Core Team. *R: A Language and Environment for Statistical Computing*; R Foundation for Statistical Computing: Vienna, Austria, 2025. Available online: https://www.R-project.org/ (accessed on 5 December 2025).
47. Martini, D.; Sakowska, K.; Wohlfahrt, G.; Pacheco-Labrador, J.; van der Tol, C.; Porcar-Castell, A.; Magney, T.S.; Carrara, A.; Colombo, R.; El-Madany, T.S.; et al. Heatwave breaks down the linearity between sun-induced fluorescence and gross primary production. *New Phytol.* **2022**, *233*, 2415–2428. [CrossRef]
48. Jia, Q.; Liu, Z.; Guo, C.; Wang, Y.; Yang, J.; Yu, Q.; Wang, J.; Zheng, F.; Lu, X. Relationship between Photosynthetic CO2 Assimilation and Chlorophyll Fluorescence for Winter Wheat under Water Stress. *Plants* **2023**, *12*, 3365. [CrossRef]
49. Nour, M.M.; Aljabi, H.R.; AL-Huqail, A.A.; Hornebur, B.; Mohammed, A.E.; Alotaibi, M.O. Drought responses andadaptation in plants differing in life-form. *Front. Ecol. Evol.* **2024**, *12*, 1452427. [CrossRef]
50. Tognetti, R.; Johnson, J.D.; Michelozzi, M. The response of European beech (*Fagus sylvatica* L.) seedlings from two Italian populations to drought and recovery. *Trees* **1995**, *9*, 348–354. [CrossRef]
51. Sellers, P.J. Canopy reflectance, photosynthesis and transpiration. *Int. J. Remote Sens.* **1985**, *6*, 1335–1372. [CrossRef]
52. Gao, X.; Huete, A.R.; Ni, W.; Miura, T. Optical–Biophysical Relationships of Vegetation Spectra without Background Contamination. *Remote Sens. Environ.* **2000**, *74*, 609–620. [CrossRef]
53. Leuschner, C. Drought response of European beech (*Fagus sylvatica* L.)—A review. *Perspect. Plant Ecol. Evol. Syst.* **2020**, *47*, 125576. [CrossRef]
54. Buddenbaum, H.; Stern, O.; Paschmionka, B.; Hass, E.; Gattung, T.; Stoffels, J.; Hill, J.; Werner, W. Using VNIR and SWIR field imaging spectroscopy for drought stress monitoring of beech seedlings. *Int. J. Remote Sens.* **2015**, *36*, 4590–4605. [CrossRef]
55. Dalponte, M.; Andreatta, D.; Coomes, D.A.; Marchesini, L.B.; Marinelli, D.; Vescovo, L.; Gianelle, D. Canopy spectral responses of temperate forests to late spring frost and hot drought events assessed with Sentinel-2 NDVI time series. *Remote Sens. Appl. Soc. Environ.* **2025**, *40*, 101737. [CrossRef]
56. Wang, R.; Gamon, J.A.; Russo, S.E.; Nishimwe, A.V.; Ellerman, H.; Wardlow, B. Multitemporal airborne imaging spectrometry and fluorometry reveal contrasting photoprotective responses of trees. *Remote Sens. Environ.* **2024**, *311*, 114295. [CrossRef]
57. Michel, A.; Haggenmüller, K.; Kirchner, T.; Prescher, A.K.; Schwärzel, K. (Eds.) Forest Condition in Europe: The 2025 Assessment. In *ICP Forests Technical Report Under the UNECE Convention on Long-Range Transboundary Air Pollution (Air Convention)*; Thünen Institute: Eberswalde, Germany, 2025; 100p. [CrossRef]
58. Thomas, F.M.; Blank, R.; Hartmann, G. Abiotic and biotic factors and their interactions as causes of oak decline in Central Europe. *For. Pathol.* **2002**, *32*, 277–307. [CrossRef]
59. Bigler, C.; Bräker, O.U.; Bugmann, H.; Dobbertin, M.; Rigling, A. Drought as an Inciting Mortality Factor in Scots Pine Stands of the Valais, Switzerland. *Ecosystems* **2006**, *9*, 330–343. [CrossRef]
60. Liepiņš, K.; Bleive, A. The Potential of European Beech (*Fagus sylvatica* L.) in the Hemiboreal Baltic Region: A Review. *Forests* **2025**, *16*, 109. [CrossRef]
61. Machar, I.; Vlckova, V.; Bucek, A.; Vozenilek, V.; Salek, L.; Jerabkova, L. Modelling of Climate Conditions in Forest Vegetation Zones as a Support Tool for Forest Management Strategy in European Beech Dominated Forests. *Forests* **2017**, *8*, 82. [CrossRef]
62. Mathes, T.; Seidel, D.; Klemmt, H.J.; Thom, T.; Annighöfer, P. The effect of forest structure on drought stress in beech forests (*Fagus sylvatica* L.). *For. Ecol. Manag.* **2024**, *554*, 121667. [CrossRef]

63. Mölder, I.; Leuschner, C. European beech grows better and is less drought sensitive in mixed than in pure stands: Tree neighbourhood effects on radial increment. *Trees* **2014**, *28*, 777–792. [CrossRef]
64. Schmied, G.; Pretzsch, H.; Ambs, D.; Uhl, E.; Schmucker, J.; Fäth, J.; Biber, P.; Hoffmann, Y.-D.; Šeho, M.; Mellert, K.H.; et al. Rapid beech decline under recurrent drought stress: Individual neighborhood structure and soil properties matter. *For. Ecol. Manag.* **2023**, *545*, 121305. [CrossRef]